

Why epithelial cells collectively move along a traveling signal wave

Tatsuya Fukuyama,^{1,*} Hiroyuki Ebata,^{2,†} Yohei Kondo,^{3,4,5}
Satoru Kidoaki,² Kazuhiro Aoki,^{3,4,5} and Yusuke T. Maeda¹

¹*Kyushu University, Department of Physics, Motooka 744, Fukuoka 819-0395, Japan*

²*Kyushu University, Institute for Materials Chemistry and Engineering, Motooka 744, Fukuoka 819-0395, Japan*

³*National Institute for Basic Biology, NINS, Higashiyama 5-1, Myodaiji-cho, Okazaki, Aichi 444-8787, Japan*

⁴*ExCELLS, NINS, Higashiyama 5-1, Myodaiji-cho, Okazaki, Aichi 444-8787, Japan*

⁵*Department of Basic Biology, SOKENDAI, 5-1 Higashiyama, Myodaiji-cho, Okazaki, Aichi 444-8787, Japan*

(Dated: June 22, 2022)

The directional collective migration along traveling signal waves is indispensable for the development in multicellular tissues. However, little is known about how the net motion occurs under wave-like activation while the forces are balanced. To reveal the law of migration with the traveling wave, we study collective migration by considering the signal-dependent coordination of contractile stress and adhesive friction to the substratum. We show that their interplay forms a non-reciprocal motion that enhances the backward motion against a signal wave. Moreover, the relaxation dynamics during this non-reciprocal motion realize a noise filter by which the migration velocity is optimized under a certain wave velocity. Our finding thus brings deep understanding of the rectified migration by a traveling signal wave, which may be involved in wound healing of epithelial tissues.

Collective cell migration is essential in embryogenesis, morphogenesis, immunological responses, and wound healing [1–5]. To develop ordered and complex structures, a group of cells responds to a traveling signal wave and correctly determines their direction of migration [6]. However, a spatially symmetrical wave produces no net motion of the cells because the forces generated across the signal wave have equal magnitude but opposite signs. Cells may utilize an apparent memory to rectify their direction while the forces are balanced [7, 8], however, such a memory effect is elusive in collective migration.

A key concept for resolving this question is the motion with the broken time-reversal symmetry, termed non-reciprocal motion [9, 10]. If the cell migration driven by internal force consists of more than two processes, the time-reversal symmetry can be broken [11–15] and net motion occurs. Hence, it is a long-standing challenge to find fundamental link between non-reciprocal motion and a traveling signal wave, which may be relevant to not only epithelial tissues [3, 5] but also active colloids [16].

In this Letter, we propose a theoretical model for collective migration along a traveling signal wave. Considering that the cell-activated signal simultaneously controls local cell contraction and adhesive friction to the substrate, we show that the damping of the friction enhances the net motion opposite to the signal wave. With experimental verifications, our model explains all key aspects such as the onset of collective migration, directionality, and the optimal response to the signal wave. We thus conclude that wave-directed migration results from the interplay of signal-dependent contraction and adhesive friction cellular mechanics.

To reveal the mechanism of how a signal wave induces non-reciprocal motion at a multicellular tissue, we consider continuum mechanics in which both the contractile force exerted by a cell and the adhesive stress on the sub-

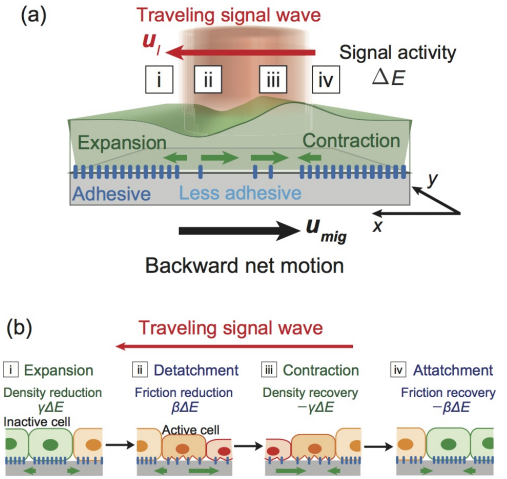


FIG. 1. Non-reciprocal motion by a traveling signal wave. (a) Schematic illustration of directed collective migration with a traveling signal wave. Signal activation causes a cell to be pulled by the surrounding cells (I: Expansion). The activated signal in turn reduces the adhesive friction between the cell and the substratum (II: Detaching). As the signal wave goes through the cell monolayer, the activated cell relaxes the pulling force (III: Contraction) and then adhere to the substratum (IV: Attaching). (b) Schematic illustration of non-reciprocal motion. Four distinct stages break the time-reversal symmetry in motion.

strate depend on the magnitude of the signal activation (Fig. 1(a)). The migration process of the cell population is driven by internal forces that maintain a force-free cycle, as a single cell does [18–21]. Given that the cell population adheres to a substratum on a two-dimensional plane under a periodic boundary condition, the contractile stress generated by the cells and the adhesive stress received from the substratum are balanced (Fig. S1). The conservation of momentum is given by $\nabla \cdot \sigma + f^{ad} = 0$

[22, 23], where the contractile stress $\boldsymbol{\sigma}$ consists of the intercellular pressure π exerted by the neighbor cells. The adhesive stress is $\mathbf{f}^{ad} = -\zeta \mathbf{u}_{mig}$, where ζ is the friction coefficient of cell-substrate adhesion per unit area and \mathbf{u}_{mig} is the migration velocity of cells. The conservation of momentum is

$$\nabla \pi + \zeta \mathbf{u}_{mig} = 0, \quad (1)$$

indicating that the spatial gradient of the contractile stresses drives the displacement of cells.

The contractile stress is stronger at the rear end of the wave, where the signal continues to be activated until the wave passes (Fig. 1(a)). The activated signal then induces the contraction of cells due to the localization of the myosin light chain in the rear edge [5]. Given that the contractile stress depends on signal activity, the local density of the cells is also regulated by the magnitude of the signal $E(\mathbf{x})$ (Fig. S2). The resultant gradient of the contractile stresses changes the local density of the cells $\rho = \rho(\mathbf{x}, t)$. The local density of the cell population follows the continuity equation:

$$\frac{\partial \rho}{\partial t} + \nabla \cdot (\rho \mathbf{u}_{mig}) = 0 \quad (2)$$

when the growth and division of cells are negligible for short time scales (≈ 30 min). However, according to Eq. (1), there is no net motion, i.e., $\int d\mathbf{x} \mathbf{u}_{mig} = 0$, even under changes in the density ρ if the friction coefficient ζ does not change with signal activation. This is because the net internal stress (the integral of $\nabla \pi$ over the cell population) must always be zero. The internal stress gradient is not sufficient on its own to drive directed net motion along a traveling signal wave.

The key concept to explain the onset of net motion is the multiplicative effect in the internal force and adhesive friction on the substrate [13, 24]. Assuming that the adhesion coefficient ζ changes with signal activation, the integral of Eq. (1) over the population is $\int d\mathbf{x} \zeta \mathbf{u}_{mig} = 0$, which allows for non-zero net motion: $\int d\mathbf{x} \mathbf{u}_{mig} \neq 0$ (Fig. 1(b)). This frictional effect motivates us to consider the signal-dependent adhesive force with the frictional coefficient $\zeta = \zeta(E)$. Eventually, the changes of the density and the frictional stress due to the signal activation are,

$$\frac{\partial \rho}{\partial E} \neq 0, \quad \frac{\partial \zeta}{\partial E} \neq 0. \quad (3)$$

Here, an activated signal $\Delta E(\mathbf{x}, t)$ propagates in one direction by $\Delta E(\mathbf{x}) = E(\mathbf{x}) - E_0 = E_l \exp(-\frac{(\mathbf{x}-u_l t)^2}{2a^2})$, where u_l and a are the velocity of the wave and the typical width of the wave, respectively. The contraction of the cell monolayer induces contractile flows at the rear edge of the signal wave while the expansion of the cell monolayer, due to the conservation of volume, drives extensile flow at the wave front. The density of the cells expands to first order according to the strength of the signal activation: $\rho = \rho_0(1 + \gamma \Delta E)$, where the compression

coefficient of the cell monolayer is $\gamma = \frac{\partial(\ln \rho)}{\partial E}$. The second ingredient is the adhesive friction with the friction coefficient $\zeta = \zeta_0(1 + \beta \Delta E)$, with the dissipation coefficient $\beta = \frac{\partial(\ln \zeta)}{\partial E}$. The variation in adhesive friction augments the extensile flow at the front edge and the contractile flow at the rear edge. This imbalance eventually creates a net motion opposite to the signal wave (Fig.1(b)).

By substituting the first order expansions of $\rho(E)$ and $\zeta(E)$ above into Eqs. (1) and (2), the migration velocity \mathbf{u}_{mig} is then solved as the product of the dissipation coefficient β for the frictional change and the deformation coefficient γ for the compressibility of the cells [25],

$$\mathbf{u}_{mig} = -\mathbf{u}_l \frac{\beta \gamma}{2} (\Delta E)^2. \quad (4)$$

Importantly, the positive sign of $\beta \gamma > 0$ signifies that the cell population migrates opposite to the signal wave.

We next examine how a traveling signal wave organizes adhesive friction and local cell density and then turns into the non-reciprocal motion. Experimental verification is performed using Madin-Darby canine kidney (MDCK) cells. It is known that in the monolayer of MDCK cells, the signal activity of ERK MAP kinase propagates like a traveling wave and drives collective migration in the opposite direction of the wave [2, 5, 26]. We first clarify whether the adhesive friction and contractile stress gradients are involved in the ERK wave-driven migration. The quantitative indicator of cellular adhesiveness is the magnitude of the traction stress (Fig. S3), which is proportional to the size of the focal adhesion. We therefore employed traction force microscopy and measured the change in the traction force after the phosphorylation of ERK MAP kinase (later ERK activation).

A single isolated MDCK cell exerted a traction stress of $F_0 = 400$ Pa (Fig. 2(a), blue). The magnitude of ERK activation ΔE was measured by the ratio of ERK-mCherry translocation into cell nucleus (Fig. S4). The stress damping began after the ERK activation with 32 nM 12-O-Tetradecanoylphorbol 13-acetate (TPA) and continued for 30 min (Fig. S4) [27]. The traction stress eventually decreased to $F = 300$ Pa (Fig. 2(a), red). The number of traction force spots where large traction stress is present was reduced to zero after the addition of TPA, indicating the reduced adhesive force on the substrate. The specificity of the ERK-induced force reduction was also investigated by a MEK inhibitor that suppresses the activated ERK signal (Fig. 2(a), green). The force reduction was not observed with the simultaneous dose of 1 μ M MEK inhibitor and 32 nM TPA. This result indicates that the reduced traction force results from the activated ERK signal, i.e. $\beta < 0$. The traction force was decreased in an ERK activity-dependent manner in a group of cells (Fig. S3), indicating the ERK signal is involved in the adhesive force of epithelial cell monolayer.

To quantify the dissipative coefficient of adhesive friction β , we measured the reduction rate of the traction

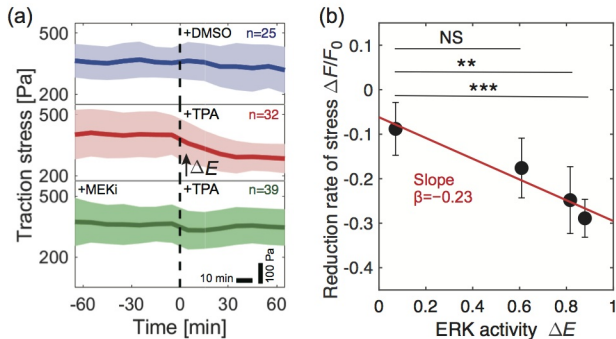


FIG. 2. The signal activation reduces the adhesive friction on the substrate. (a) Time evolution of traction force in single MDCK cells. Chemical activation by 32 nM TPA was performed at time $t = 0$ min. Top: control group (blue, DMSO), middle: ERK activation group (red, TPA), Bottom: ERK suppression group (green, TPA and MEK inhibitor). The solid line represents the average value, and the region in pale color represents the standard deviation. (b) The traction force at various levels of signal activation with 1.0 nM (56% ERK activation), 3.2 nM (81% ERK activation), and 32 nM (88% ERK activation). Statistical analysis was done by U-test; ** denotes $p < 0.01$ significance.

stress $\Delta F/F_0$ by using partial signal activation at various concentrations of TPA (Fig. 2(b)). The reduction rate of the traction stress was almost proportional to the strength of the activated signal. Considering that the reduction rate of the traction stress corresponds to the magnitude of the decrease in the adhesion, the dissipation coefficient is $\beta \approx \frac{1}{\Delta E} \frac{\Delta F}{F_0} = -0.23$.

Another signal-dependent mechanism to be verified is the change in cell density. We analyzed the change in local cell density by using optogenetic activation of ERK MAP kinase. We chose an MDCK cell strain with the ability to activate an ERK signal with light-induced dimerization (LID) of CRY2-CIBN [3, 5] (Fig. S5). We built a mixed cell population in which a small fraction (10%) of the MDCK cells activated by light was surrounded by the rest (90%) of other MDCK cells that do not respond to light (Fig. 3(a)). After light-induced ERK activation for 30 min, the activated cells exhibited a significant increase in area (Fig. 3(b)), suggesting that the activated cell was stretched by the stress across the activated and non-activated cells since the surrounding cells maintain adhesion. In contrast, for isolated single cells (Fig. 3(c)), the ERK activation did not affect the cell area (Fig. 3(d)). These results indicate that local ERK activation builds the gradient of intercellular stress and in turn reduces the cell density, i.e. $\gamma < 0$.

Furthermore, Eq. (4) indicates that the velocity of cell migration is proportional to the square of ERK activity, i.e., $u_{mig} \propto (\Delta E)^2$, and this squared relationship means that the two processes are multiplicatively involved. We decided to test this by using a

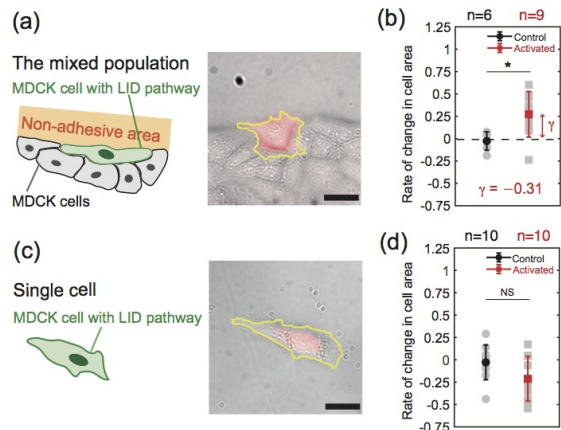


FIG. 3. The signal activation reduces the density of the cells. (a) Schematic illustration of a single cell with light inducible dimerization (LID) pathway in the mixed cell population. Red color represents ERK-mCherry. (b) Changes in the area of the ERK-activated cells in the mixed cell population. The area of the ERK-activated cells was analyzed from the images. Statistical analysis was done by U-test; * denotes $p < 0.05$ significance. (c) Representative image of an isolated single cell with the LID pathway. (d) Changes in cell area in isolated single cells. Scale bars: 30 μm .

synthetic ERK wave that recapitulates the signal wave by sweeping blue light in one direction (Fig. S6) [5]. We swept the synthetic ERK wave at a constant velocity $u_l = 2.0 \mu\text{m}/\text{min}$, and its activity ΔE was controlled by the laser intensity. The migration speed $|u_{mig}|$ increased with the square of the ERK activity $(\Delta E)^2$ (Fig. 4(b)), which is in agreement with Eq. (4). Furthermore, substituting the experimental values of the dissipation coefficient $\beta = -0.23$ and the deformation coefficient $\gamma = -0.31$ (Fig. 2(b) and Fig. 3(b), respectively) into Eq. (4) with $\Delta E = 0.88$, the speed of migration is $u_{mig} \approx -0.11 \mu\text{m}/\text{min}$ when the wave velocity is $u_l = 2.9 \mu\text{m}/\text{min}$. This shows good agreement with the experimental value of $u_{mig} \approx -0.20 \mu\text{m}/\text{min}$.

An unique property of directed motion driven by signal waves is the existence of an optimal wave velocity that maximizes the velocity of the motion [5, 7, 16]. Examining the relation between the speed of signal waves and collective migration can reveal how cells respond to time-varying signals by utilizing non-reciprocal motion. We thus measured the dependence of the migration velocity on the wave speed; Fig. 4(c) shows the maximum migration velocity $u_{mig} = -0.2 \mu\text{m}/\text{min}$ at an intermediate wave speed $u_l = 2.3 \mu\text{m}/\text{min}$.

Since cell migration proceeds with repeating deformation and restoration, viscoelastic deformation is involved in the cycle of non-reciprocal motion. The extended deformation coefficient is $\Gamma_\tau = \gamma \left[1 - \exp\left(-\frac{\lambda}{u_l \tau}\right) \right]$ [25], where τ is the characteristic time of mechanical restoration ($\tau \approx 4$ min [28]), λ is the wavelength of the traveling

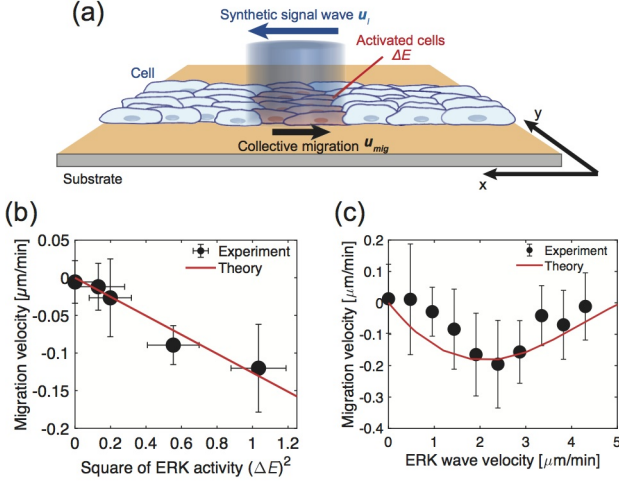


FIG. 4. Non-reciprocal motion determines the migration velocity, direction, and optimal wave speed. (a) Collective migration by a sweeping synthetic ERK wave. The cell monolayer having the L1D pathway was patterned into a channel-shape of width $500\ \mu\text{m}$. A spot of blue light moves along the channel-patterned cell monolayer at a velocity u_l . (b) Squared dependence of the migration velocity on the magnitude of the synthetic ERK wave. The solid curve illustrates Eq.(4). (c) Optimal speed of a synthetic ERK wave. The migration has the maximum velocity at an intermediate speed of the ERK wave (black circles). Theoretical curve Eq. (5) with the mechanical relaxation time of $\tau = 4\ \text{min}$ [28] fits experimental data (solid red line).

wave of ERK activation ($\lambda = 450\ \mu\text{m}$ [3, 5]). By considering the characteristic times of density change and the instantaneous change of adhesion (Fig. 2(a)) [29], the migration velocity u_{mig} is extended to a general form:

$$u_{mig} = -u_l \frac{\beta \Gamma_\tau}{2} (\Delta E)^2. \quad (5)$$

For a slow signal wave $u_l/\lambda \ll 1/\tau$, the migration velocity u_{mig} increases linearly with the wave velocity u_l according to $u_l(1 - \exp[-\lambda/(u_l\tau)]) \sim u_l$. In contrast, for a fast signal wave $u_l/\lambda \gg 1/\tau$, the velocity of the collective movement plateaus as $u_l(1 - \exp[-\lambda/(u_l\tau)]) \sim 1/\tau$.

To explain the optimality of u_{mig} , we have to consider another relaxation process for a slow signal wave, that is, the decay of signal activity. The activated signal decays over time according to the relaxation constant $\tau_E \approx 10\ \text{min}$ [3]. The duration of the signal activation is close to the time scale of the ERK wave propagation $T \approx b/u_l$ with a typical cell size of $b = 20\ \mu\text{m}$. If the activation time T is sufficiently longer than the relaxation time ($T \gg \tau_E$), non-reciprocal motion due to ERK activation can be induced. On the other hand, when the activation time is shorter than the relaxation time ($T \ll \tau_E$), that is, when the wave moves faster, the increase in contractile stress and reduction in adhesive friction are not sufficient. Then, the wave speed becomes optimal at about $u_l = 2 \sim 3\ \mu\text{m}/\text{min}$, which is comparable to the experimental value $2.3\ \mu\text{m}/\text{min}$ (Fig. 4(c)).

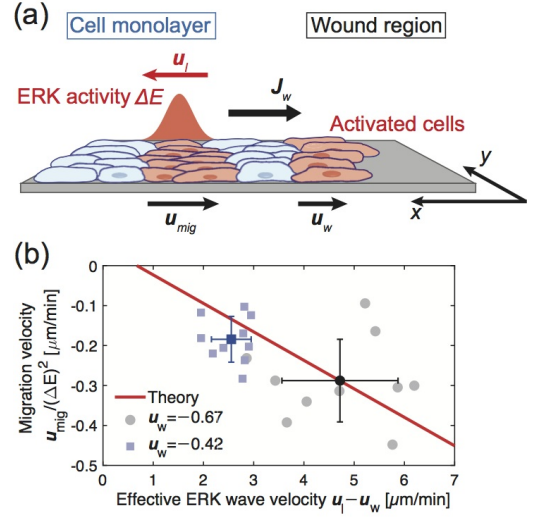


FIG. 5. Collective migration in a traveling ERK wave during wound healing. (a) Model of collective motion in the ERK wave in wound healing. (b) The correlation between migration speed and the speed of the ERK wave. We plot the data in different colors taken on two independent experiments. Each data point corresponds to directed migration under one ERK wave. The solid line represents Eq.(6) with $\beta = -0.23$ (estimated from Fig. 2) and $\gamma = -0.31$ (Fig. 3).

We finally examine how our theoretical model can be extended to wound healing of cell monolayer (Fig. 5(a)) [30]. In epithelial tissues, the signal wave propagates from the wound at velocity u_l , and the activated signal of ERK wave travels [3, 5, 26]. The cells collectively move toward the wound region and then fill the gap. Given that the edge of the wound region moves at a constant speed u_w , the flux of the cell density $\mathbf{J}_w = \rho \mathbf{u}_w$ occurs at the leading edge. Since the boundary that generates the signal wave moves in the opposite direction, Eq. (2) is rewritten by $\frac{\partial \rho}{\partial t} + \nabla \cdot (\rho \mathbf{u}_{mig}^{wh}) = \nabla \cdot \mathbf{J}_w$. At the moving frame of a traveling signal wave, the flux of cell density yields $-(u_l - u_w) \frac{d\rho}{dx} + \rho \frac{d\mathbf{u}_{mig}^{wh}}{dx} = 0$, which indicates the effective velocity of the signal wave is $u_l - u_w$. The migration velocity Eq. (5) is therefore extended as

$$u_{mig}^{wh} = -\frac{u_l - u_w}{2} \beta \Gamma_\tau (\Delta E)^2. \quad (6)$$

The scaled migration velocity $u_{mig}^{wh}/(\Delta E)^2$ was plotted as the effective velocity of the ERK wave, $u_l - u_w$ (Fig. 5(b)). The data from two independent experiments overlaps the theoretical curve of Eq. (6) with $\beta = -0.23$ and $\gamma = -0.31$ (Fig. 5(b)), showing good agreement with the model of non-reciprocal motion by the ERK wave.

In conclusion, the coordination of changes in the adhesive friction and contractile stresses can induce net collective motion counter to a traveling signal wave. Around the rear end of the signal wave, the friction coefficient decreases, and the contractile stress increases. As a result, the pulling force from the rear end drives the net

backward motion of the cells. On the other hand, at the front end of the wave, the cells are stretched due to the conservation of volume, which emphasizes the velocity of motion opposite to the wave.

Two important parameters $\beta = -0.29$ (adhesive friction) and $\gamma = -0.31$ (density change by contraction) in Eq. (4) can also be evaluated from the friction coefficient and elastic modulus of epithelial cells obtained in previous studies [25, 31–33]. For typical epithelial cells, the friction coefficient per unit area is $\zeta \approx 15 \text{ Pa min}/\mu\text{m}^2$ [31, 32] and the contractile stress is $\sigma \approx 400 \text{ Pa}$ (Fig. 2). When cells move at $u_{mig} \approx 0.2 \mu\text{m}/\text{min}$ with the ERK activation $\Delta E = 1.0$, Eq. (1) gives $|\beta| \approx \frac{\zeta u_{mig}}{\sigma/b - \zeta u_{mig}} \approx 0.2$. In addition, the elastic modulus of MDCK cells is $G \approx 1 \text{ kPa}$ [33], and the coefficient of compressibility also shows good agreement with $|\gamma| \approx \sigma/G \approx 0.4$.

The essence of this non-reciprocal motion is to utilize the phase difference of the two coordinated periodic processes of adhesive friction and contractile stress while keeping force-balance [11, 13, 21]. By including another degree of control in addition to the contractile stresses, cells can control the direction of collective motion by adjusting the sign of the phase difference between the two periodic processes. Recent reports have shown that the contractile stress and polarity of epithelial cells [5, 17, 26] are involved in persistent collective migration. The simple rule only from measured values is indispensable for controlling of collective migration based on mechanics. The further understanding of mechanical coordination of contraction and friction, including force-signaling feedback [34], may bring physical insights in the broad spectrum of active dynamics organized by a traveling waves.

This work was supported by Grant-in-Aid for Scientific Research on Innovative Areas (16H00805, 17H05234 and 18H05427 to YTM, 19H05798 to KA) and Grant-in-Aid for Scientific Research (B) (17KT0025 and 20H01872 to YTM, 18H02444 to KA) from MEXT, and CREST JST Grant (JPMJCR1654) to KA, AMED-CREST Grant (JP20gm0810002) to SK, and NIBB Collaborative Research Program (18-355) to YTM.

* fukuyama@phys.kyushu-u.ac.jp

† ebata@ms.ifoc.kyushu-u.ac.jp

- [1] P. Friedl and D. Gilmour, *Nat. Rev. Mol. Cell Biol.* **10**, 445-457 (2009).
 [2] Y. Matsubayashi, M. Ebisuya, S. Honjoh, and E. Nishida, *Curr. Biol.* **14**, 731-735 (2004).
 [3] K. Aoki, Y. Kumagai, A. Sakurai, N. Komatsu, Y. Fujita, C. Shionyu, and M. Matsuda, *Mol. Cell* **52**, 529-540 (2013).
 [4] T. Hiratsuka, Y. Fujita, H. Naoki, K. Aoki, Y. Kamioka, and M. Matsuda, *eLife* **4**, e05178 (2015).
 [5] K. Aoki, Y. Kondo, N. Honda, T. Hiratsuka, R.E. Itoh, and M. Matsuda, *Dev. Cell* **43**, 305-317 (2017).

- [6] C. Londono, M.J. Loureiro, B. Slater, P.B. Lucker, J. Soleas, S. Sathananthan, J.S. Aitchison, A.J. Kabla, and A.P. McGuigan, *Proc. Natl Acad. Sci. U.S.A.* **111**, 1807-1812 (2014).
 [7] A. Nakajima, S. Ishihara, D. Imoto, and S. Sawai, *Nat. Commun.* **5**, 5367 (2014).
 [8] M. Skoge, H. Yue, M. Erickstad, A. Bae, H. Levine, A. Groisman, W.F. Loomis, and W.-J. Rappel, *Proc. Natl Acad. Sci. U.S.A.* **111**, 14448-14453 (2014).
 [9] E.M. Purcell, *Am. J. Phys.* **45**, 3-11 (1977).
 [10] A. Najafi and R. Golestanian, *Phys. Rev. E* **69**, 062901 (2004).
 [11] K.V. Kumar, S. Ramaswamy, and M. Rao, *Phys. Rev. E* **77**, 020102(R) (2008).
 [12] T. Qiu, T.-C. Lee, A.G. Mark, K.I. Morozov, R. Munster, O. Mierka, S. Turek, A.M. Leshansky, and P. Fischer, *Nat. Commun.* **5**, 5119 (2014).
 [13] E. Lauga, *Soft Matt.* **7**, 3060-3065 (2011).
 [14] M. Leoni and P. Sens, *Phys. Rev. Lett.* **118**, 228101 (2017).
 [15] M.H. Mai and B.A. Camley, *Soft Matt.* **16**, 1349-1358 (2020).
 [16] C. Lozano and C. Bechinger, *Nat. Commun.* **10**, 2495 (2019).
 [17] S. Jain, *et al.* *Nat. Phys.* **16**, 802-809 (2020).
 [18] S. Wang and P.G. Wolynes, *Proc. Natl. Acad. Sci. U.S.A.* **108**, 15184-15189 (2011).
 [19] H. Tanimoto and M. Sano, *Biophys. J.* **106**, 16-25 (2014).
 [20] H. Ebata, K. Moriyama, T. Kuboki, and S. Kidoaki, *Biomaterials* **230**, 119647 (2020).
 [21] M. Tarama and R. Yamamoto, *J. Phys. Soc. Japan* **87**, 044803 (2018).
 [22] S. Banerjee, K. J. C. Utuje, and M.C. Marchetti, *Phys. Rev. Lett.* **114**, 228101 (2015).
 [23] S. Yabunaka and P. Marcq, *Soft Matt.* **13**, 7046-7052 (2017).
 [24] T. Fukuyama, S. Nakama, and Y.T. Maeda, *Soft Matt.* **14**, 5519-5524 (2018).
 [25] Theoretical details and experimental methods are fully described in supplemental information.
 [26] N. Hino, L. Rossetti, A. Marín-Llauradó, K. Aoki, X. Trepat, M. Matsuda, T. Hirashima, *Dev. Cell* **53**, 646-660 (2020).
 [27] A. Sharma, C. T. Luke, N. A. Dower, J. C. Stone, and P. S. Lorenzo, *J. Biol. Chem.* **285** 15724-15730 (2010).
 [28] K.V. Iyer, R. Piscitello-Gomez, J. Pajmians, F. Julicher, and S. Eaton, *Curr. Biol.* **29**, 578-591 (2019).
 [29] A. Hamadi, M. Bouali, M. Dontenwill, H. Stoeckel, K. Takeda, and P. Ronde, *J. Cell Sci.* **118**, 4415-4425 (2005).
 [30] M. Basan, J. Elgeti, E. Hannezo, W.-J. Rappel, and H. Levine, *Proc. Natl. Acad. Sci. U.S.A.* **110**, 2452-2459 (2013).
 [31] O. Cochet-Escartin, J. Ranft, P. Silberzan, and P. Marcq, *Biophys. J.* **106**, 65-73 (2014).
 [32] G. Duclos, C. Blanch-Mercader, V. Yashunsky, G. Salbreaux, J.-F. Joanny, J. Prost, and P. Silberzan, *Nat. Phys.* **14**, 728-732 (2018).
 [33] Y. Fujii, Y. Ochi, M. Tuchiya, M. Kajita, Y. Fujita, Y. Ishimoto, and T. Okajima, *Biophys. J.* **116**, 1152-1158 (2019).
 [34] D. Boockock, N. Hino, N. Ruzickova, T. Hirashima, and E. Hannezo, *bioRxiv* 096479 (2020).